JOURNAL OF MATERIALS SCIENCE 29 (1994) 3906–3912

The influence of temperature on the mechanical and fracture properties of a 20 vol% ceramic particulate-reinforced aluminium matrix composite

MOHAMMED JAFAR HADIANFARD, JOSEPH HEALY, YIU-WING MAI*
Centre for Advanced Materials Technology, Department of Mechanical and Mechatronic Engineering, University of Sydney, New South Wales 2006, Australia

The influence of test temperature on the mechanical and fracture properties of a 20 vol% alumina particulate-reinforced 6061-aluminium matrix composite, in the peak-aged condition, was investigated in the temperature range 25–180 °C. Strength and stiffness were found to decrease but elongation to failure increased with increasing test temperature. However, the fracture toughness was relatively constant over this temperature range. The failure mechanism, the reaction zone around reinforcing particles, the number of debonded particles and void sizes were all significantly influenced by temperature. The role of the matrix/particle interface in the fracture process was also investigated.

1. Introduction

Discontinuously reinforced metal matrix composites (MMCs) have considerable potential for applications in the aerospace industry because of their superior stiffness, higher specific mechanical properties, better dimensional stability and strength retention at elevated temperatures when compared to their monolithic counterparts. The elevated temperature application of metal matrix composites is dependent on the degree of thermal degradation of their mechanical properties. While particulate-reinforced metal matrix composites present better strength at elevated temperature than their corresponding unreinforced alloys [1], their fracture properties have been reported to depend on test temperature [2]. For example, Somerday *et al.* [3] observed that the fracture toughness of a 2XXX aluminium alloy reinforced with silicon carbide (SiC) particles increased monotonically from 18 MPa $m^{1/2}$ to 29 MPa $m^{1/2}$ in the temperature range 25–220 °C. Further increase in temperature caused a reduction in toughness to as low as 14 MPa $m^{1/2}$ at 316 °C. An investigation of the fracture mechanisms of an alumina-reinforced aluminium showed that preferred void nucleation sites changed from the interface with flat areas normal to the applied stress to those sites exhibiting a sharp corner in the direction of the stress axis as the test temperature was increased [4].

The properties of metal matrix composites are strongly influenced by the nature of the bonding between the reinforcement phase and matrix alloy, and the effect of test temperature on their microstructure. The importance of the interface increases as the reinforcement size decreases [5]. A decrease in particle size for a given volume fraction increases dramatically the contact area between the matrix and the reinforcement particles. Thus the number of atoms at the interface is increased in comparison to those in the bulk. Exposure to and/or tests conducted at elevated temperature may affect the interface bond strength and subsequently alter the mechanical properties of the MMCs. Hence, Kim *et al.* [6] found a general decrease in transverse tensile strength with increasing time of exposure at 500 °C. Although there has been some published work on the effect of temperature on the fracture and mechanical properties of metal matrix composites, experimental data are still limited [1–4]. This study investigated the elevated temperature mechanical behaviour of a particulate-reinforced aluminium metal matrix composite with a view to extend the operating temperature range of MMCs.

2. Experimental procedure

2.1. Material

The material used in this study was Comral-85, a 6061-aluminium alloy containing 20 vol% microsphere alumina particulate. It was produced by a liquid metallurgy process, and supplied by Comalco Research Centre, Thomastown, Australia. The matrix alloy contains Al–0.8Mg–0.6Si [7], and a microsphere reinforcement phase of polycrystalline material consisting of α-alumina and mullite ($Al_6Si_2O_{13}$) [8]. The microspheres range in size from 3–50 μm, with an average diameter of 17.5 μm. Figs 1 and 2 show the

* On leave at the Department of Mechanical Engineering, Hong Kong University of Science and Technology, Clear Water Bay, Kowloon, Hong Kong.

0022–2461

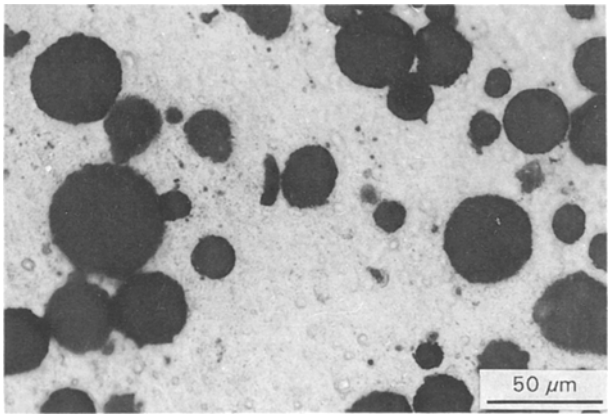

Figure 1 Microstructure of Comral-85.

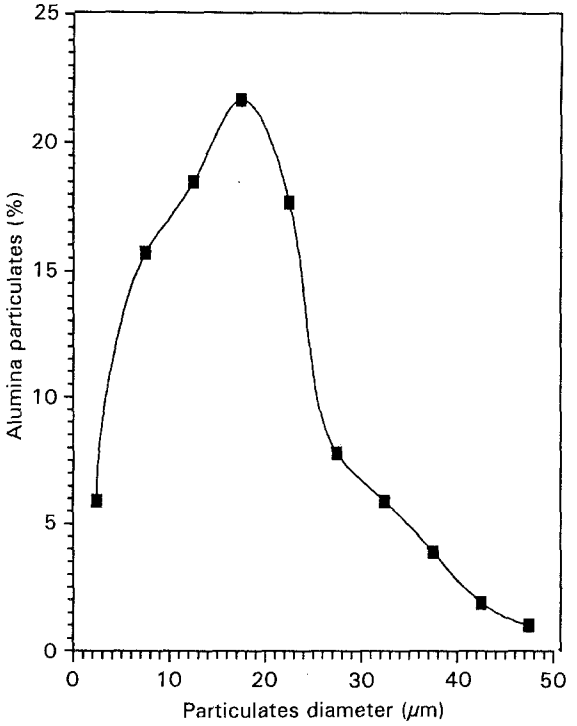

Figure 2 Particle-size distribution of Comral-85.

microstructure and particle-size distribution of Comral-85, respectively. The material was supplied in the form of extruded plates, 75 mm wide and 12 or 25 mm thick. The test specimens were heat treated to the peak-aged (T6) condition using the following heat treatment: (a) solution heat treated at 530 °C for 1.5 h, (b) cold-water quenched, (c) naturally aged for 24 h; and (d) age hardened at 175 °C for 8 h. One specimen was under-aged (UA) at 175 °C for 2 h, for comparison purposes.

2.2. Tensile and fracture toughness tests

Test specimens, with a cross-section of 11.5 mm by 12.5 mm and a gauge length of 50 mm were machined with the tensile axis parallel to the extrusion direction. The tensile tests were conducted on an 1195 Instron machine with a crosshead speed of 1 mm/min^{-1} at temperatures of 25, 100 and 180 °C. Each specimen was heated to the required temperature in approximately 30 min and allowed to stabilize for another 20 min prior to testing. The load–elongation curves were recorded by a computer-based data acquisition system. The Young's modulus, E, 0.2% offset yield, elongation to failure, ε_f, and ultimate tensile strength, UTS, were obtained for all specimens. Three specimens were tested at each temperature.

Fracture toughness tests were carried out on compact tension (CT) specimens with a width of 50 mm, machined from an extruded plate in the L–T orientation, according to the ASTM standard E399. The test specimens were fatigue precracked at room temperature in a 1603 Instron electro magnetic resonator and fractured in the 1195 Instron machine with a crosshead speed of 0.5 mm/min^{-1} at 25, 50, 100, 150 and 180 °C. The precracked specimens were heated in a similar fashion to the tensile specimens, and again three specimens were tested at each temperature.

2.3. Fractography and image analysis

The fracture surfaces on the CT specimens were examined with 505 Phillips and JSM Jeol scanning electron microscopes (SEM) with energy dispersive analysis X-ray (EDAX) capability. The micrographs obtained were subjected to image analysis to identify the failure mechanisms. A computer-controlled image analyser was used to determine the void-size distribution, the number of fractured and debonded particles, size distribution and area of reinforcement particles on the fracture surfaces. A minimum of seven fields from different points on the fracture surface were examined, with approximately 250 particles measured for each specimen.

2.4. Microstructural examination

Specimens of as-received and heat-treated materials were polished to a 1 μm finish. The general features of the microstructure, e.g. particulate distribution, second-phase size and distribution were studied by optical microscopy after etching with a solution of 1% hydrofluoric acid (HF). A solution of 2% nitric acid, 0.5% HF and 97.5% ethanol was used as an enchant to facilitate investigations of the particle/matrix (m/p) interface by optical and high-resolution scanning electron microscopy, using a Jeol JSM-6000F SEM. This investigation was confined to the UA and T6 conditions and a CT specimen which had been fractured at 180 °C (CT180). Element distribution maps and semi-quantitative element analysis around the m/p interface were studied by X-ray mapping and energy dispersion spectroscopy (EDS).

2.5. X-ray diffraction analysis

The microchemistry of phases in the CT specimens which had been fractured at room temperature (CT25) and 180°C (CT180) was studied with a Siemens Diffraktometer D5000 using polished specimens $12 \times 30 \times 65$ mm^3. A 40 kV accelerating voltage and angle (2θ) of between 10° and 110° was used, with an interval of 0.04° and time of 3 s for each interval. A repeat test at the same accelerating voltage but with the angle

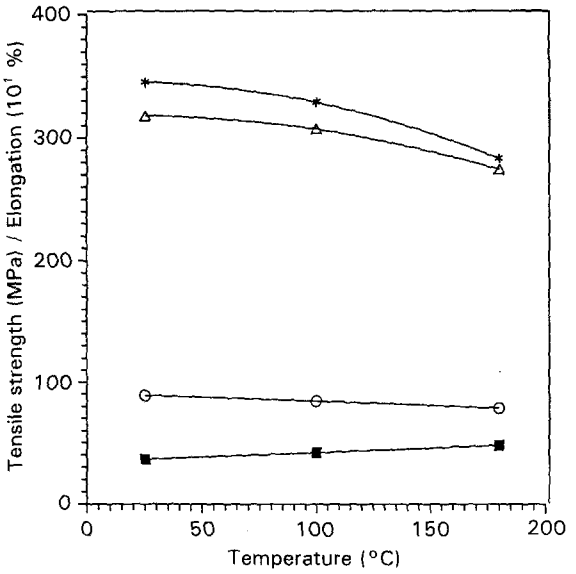

Figure 3 Variation of tensile properties of Comral-85 (T6 condition) with temperature. (*) Tensile strength (Δ) yield strength, (■) elongation to failure and (○) Young's modulus (GPa).

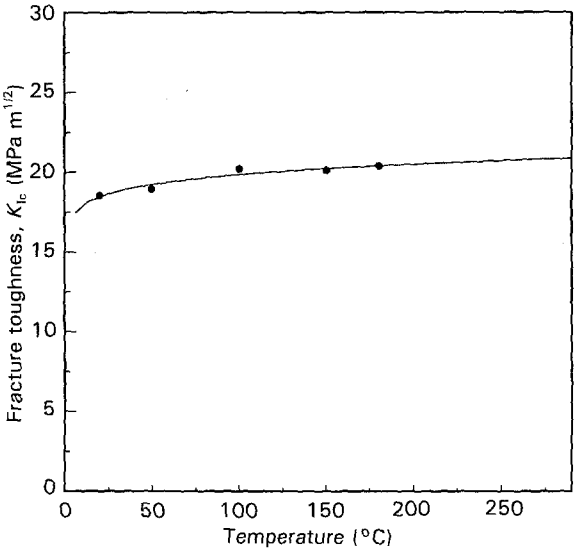

Figure 4 Variation of fracture toughness with temperature for Comral-85 (T6 condition).

reduced to between 16° and 66°, and the time for each interval increased to 6 s, was also carried out.

3. Results

3.1. Tensile and fracture toughness properties

The temperature dependence of the tensile properties of Comral-85 (T6 condition) is shown in Fig. 3. Tensile strength, UTS, 0.2% offset yield, σ_{ys}, and elastic modulus decrease with increasing temperature from 25–180 °C by 18.2%, 13.8% and 12%, respectively. However, the elongation to failure increased by 31% in this temperature range.

The variation of fracture toughness, K_{Ic}, with temperature is shown in Fig. 4. There is a marginal increase from 18.7 MPa $m^{1/2}$ at 25 °C to 20.2 MPa $m^{1/2}$ at 180 °C. Therefore, the fracture toughness of Comral-85 is relatively insensitive to temperature in the range 25–180 °C.

3.2. Fractography and image analysis

Scanning electron micrographs of the CT fracture surfaces tested at temperatures of 25, 100 and 180 °C are shown in Fig. 5a–c, respectively. The fracture surfaces are populated by numerous deep and shallow dimples and exhibit a ductile failure mode for all specimens. It would appear that in all cases the final fracture has occurred through void coalescence. The results of quantitative image analysis are listed in Table I.

The fracture surface of a specimen in the T6 condition tested at 25 °C (CT25) is covered by a large number of shallow primary dimples and many small shallow microvoids in the matrix, Fig. 5a. Three different populations of void sizes were observed on the fracture surface of this specimen, with average diameters of 16.9, 6.7 and 1.5 μm, respectively. The ligament between the primary voids was filled with secondary voids. The percentage of fractured particles

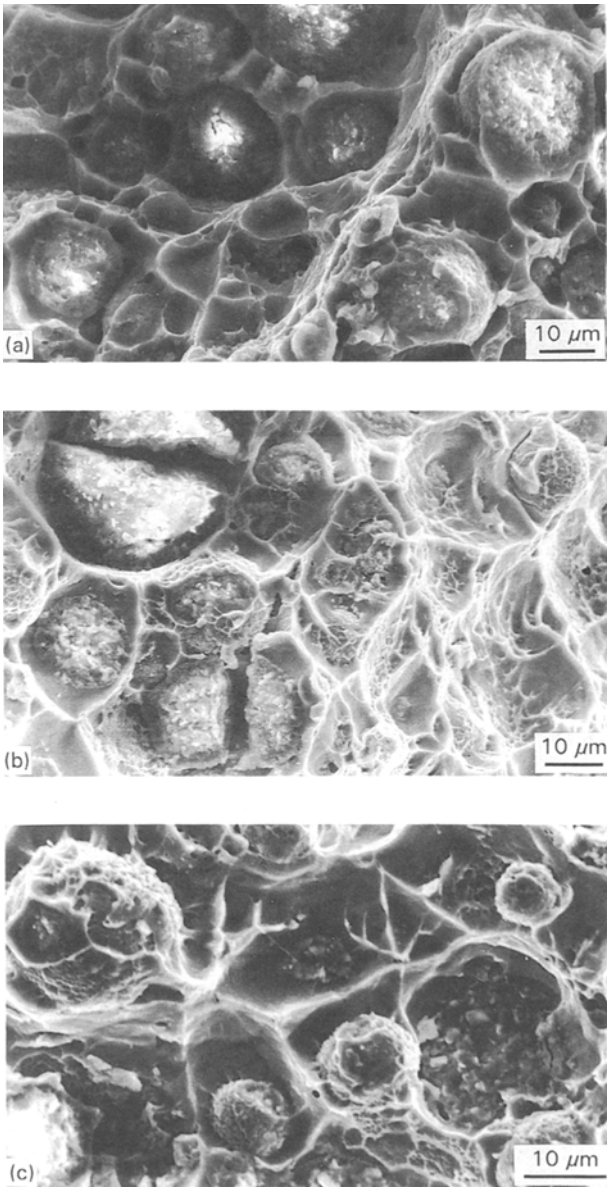

Figure 5 Scanning electron micrographs from CT fracture surfaces for Comral-85 (T6 condition) tested at (a) 25 °C; (b) 100 °C and (c) 180 °C.

TABLE I Image analysis results

Test temperature (°C)	Average particle diameter (μm)		Void diameter (μm)		Debonded particles at the m/p interface (%)	Fractured particles (%)
	Total	Fractured particles	I	II		
25	13.6	19.8	16.9	6.7	60	40.0
100	18.9	20.3	17.5	6.2	63.5	36.5
180	18.1	20.7	20.6	5.7	68.5	31.7

in CT25 was 9.3% higher than CT180 and fewer debonded particles from the m/p interface were detected.

In contrast, the fracture surface of a specimen tested at 100 °C (CT100) was covered with both large and small shallow voids, Fig. 5b. Although the percentage of debonded particles from the m/p interface in this specimen was higher than CT25, it was slightly lower than the percentage of debonded particles in CT180 (63.5% compared to 68.3%).

The fracture morphology of the CT180 specimen is characterized primarily by large deep voids around large debonded particles, with some secondary void growth observed in the matrix ligament between the reinforcement (see Fig. 5c). Individual voids can be seen, separated from each other by a thin edge of matrix at the point of final separation. This thin edge separation of voids is indicative of the high level of ductility of the matrix. The fracture surface has two sizes of dimples, one with an average diameter of 20.6 μm and the other consisting of smaller dimples with an average diameter of 5.7 μm. Two populations of damaged particles on the fracture surface of the CT180 were determined; 31.7% of the particles were fractured with an average diameter of 20.7 μm that covered about 6.9% of the fracture surface area and 68% of the particles were separated from m/p interface with an average diameter of 16.6 μm.

3.3. Microstructural examination

Fig. 1 shows the microstructure of Comral-85. A large number of secondary particles were observed on the surfaces of polished and etched specimens. The distribution and size of these particles were non-uniform and independent of heat treatment. EDS analysis showed that they consisted mainly of aluminium, iron and silicon with a small amount of chromium.

Fig. 6 is an optical micrograph of a specimen, chemically etched with a mixture of ethanol, HNO_3 and HF, showing the m/p interface. The thickness of the reaction zone is very small and microstructural details cannot be resolved by optical means. Similar reaction zones were observed for both the UA and T6 materials and all fractured specimens irrespective of test temperature. The reaction zone is irregular in cross-section, and large variations in its thickness are common from one particle to another, or even at different points of the same particle.

A high-resolution scanning electron micrograph clearly reveals the structure of interface reaction zone with its thickness (Fig. 7a). There is complete bonding between the particles and the matrix in all specimens. The reaction zone appears to consist of two layers whose thickness changes from one condition to another. EDS analysis shows the interaction zone to compose mainly of aluminium, magnesium, silicon and oxygen elements. The amount of magnesium and oxygen were higher in the layer adjacent to the particle than the layer adjacent to the matrix. The reaction zone for the under-aged sample was clean, but some small precipitates were seen in the reaction zones of the CT25 and CT180 specimens, Fig. 7b. EDS analysis of these particles showed that they were mainly composed of elements of aluminium, magnesium and silicon. The same precipitates were detected in the middle of secondary voids on the fracture surfaces of CT25 and CT100.

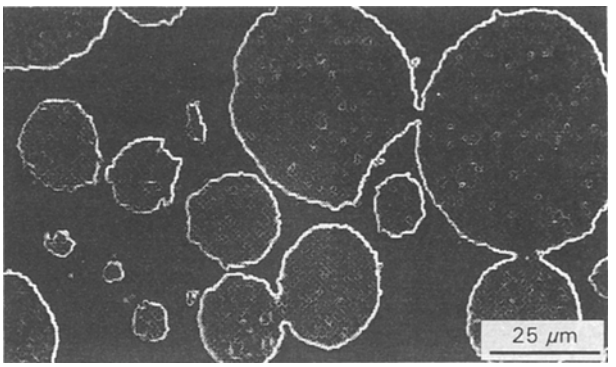

Figure 6 Optical micrograph showing m/p interface of Comral-85 (T6 condition).

Large differences in magnesium and oxygen composition exist between the interface reaction zone and neighbouring areas. Fig. 8 shows the EDS line analysis of magnesium and oxygen from the centre of one alumina particle to the centre of another, across the interface reaction zone. This figure illustrates how the concentration of these elements changes markedly at the interface layer. Therefore, it is possible to measure reaction zone size with the line analysis results and high-resolution SEM images. The average thickness of the UA reaction zone was about 0.38 μm, for CT25 and CT180 in the peak-aged condition it was 0.43 and 0.51 μm, respectively.

3.4. X-ray diffraction analysis (XRD)

The phases identified by XRD in the CT25 and CT180 (T6 condition) specimens are listed in Table II. XRD results showed the same diffraction pattern for these two specimens, although there were differences in the

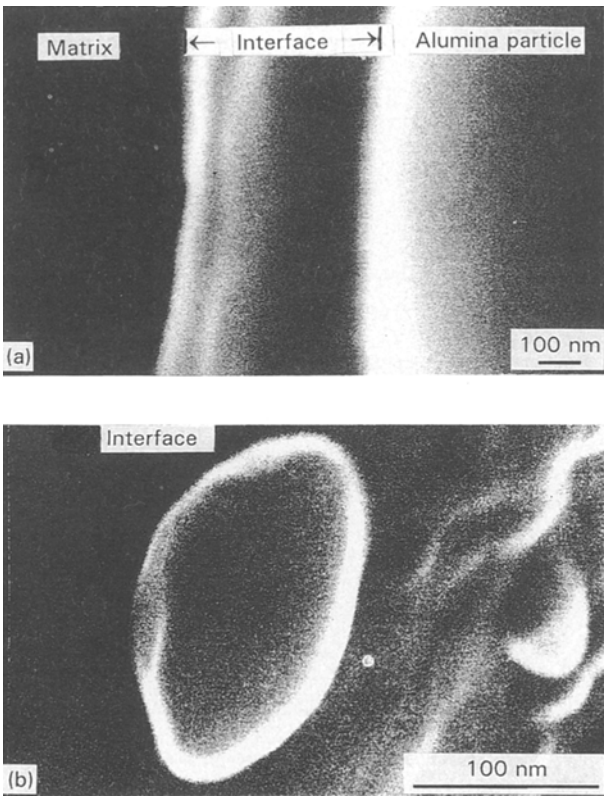

Figure 7 High-resolution scanning electron micrographs showing (a) a clean m/p interface and, (b) a secondary particle in the m/p interface.

intensity of some peaks. The peak intensity of spinel ($MgAl_2O_4$) was much higher at 180 °C (Fig. 9), as was the peak intensity of Mg_2Si. Quantitative analysis by XRD revealed that the relative amounts of spinel and Mg_2Si are also higher at 180 °C than at 25 °C.

4. Discussion

Fig. 4 indicates that the effect of temperature up to 180 °C on the fracture toughness of Comral-85 is small. A decrease of elastic modulus and strength and an increase in elongation to failure are other effects in this temperature range.

Fractographic results have shown that crack initiation and growth originates from localized plastic deformation of the matrix that produces dimple-like features typical of microvoid nucleation, growth and coalescence. This failure mode is observed for all temperatures. The dimples are relatively well formed considering the high volume fraction of reinforcement phase in the composite. Although the overall surface topography of the samples were generally unaffected by temperature, the average dimple size increased and the amount of fractured alumina particles on the fracture surface decreased with increasing temperature (see Table I) while the number of debonded particles was substantially increased.

Previous studies have addressed such factors as the deformation characteristics of the matrix and the properties of the m/p interface and their influence on the fracture behaviour of MMC composites [9, 10]. During crack initiation and growth, the particulates may fracture within the plastic zone and/or debond at

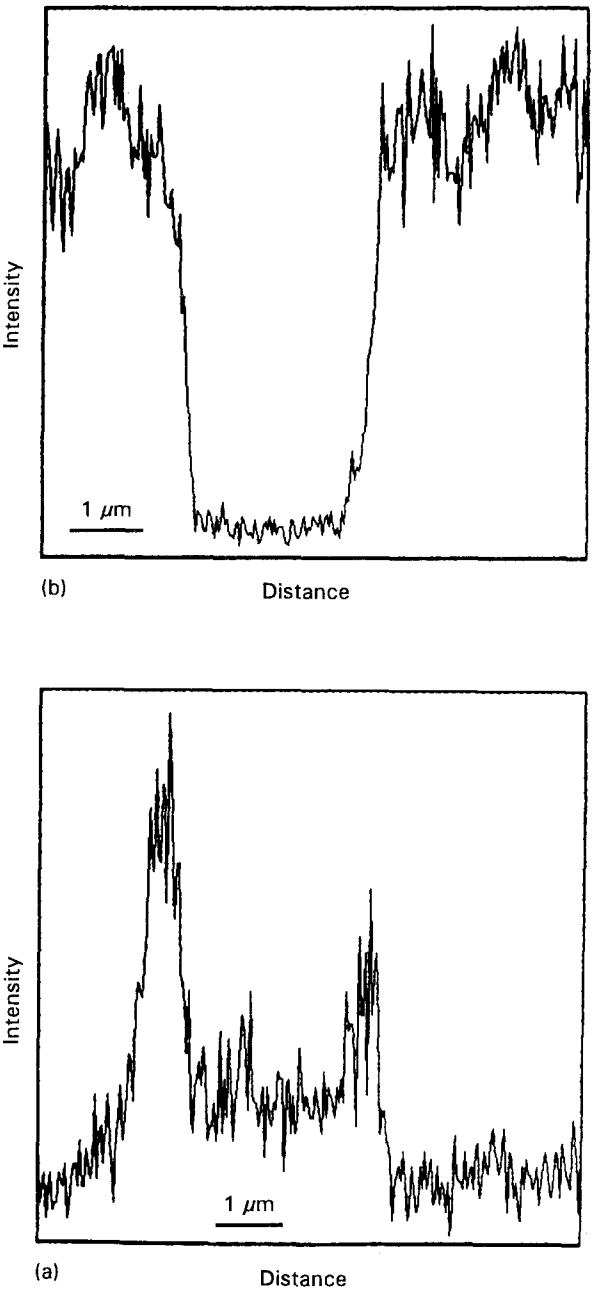

Figure 8 EDS analysis of (a) magnesium and (b) oxygen across the interface reaction zone.

TABLE II Phases existing in Comral-85

Formula of phase	Name
Al	Aluminium alloy (solid solution)
Al_2O_3	Alumina (α)
$Al_6Si_2O_{13}$	Mullite
$MgAl_2O_4$	Spinel
Mg_2Si	Magnesium silicate
$FeSiAl_5$	–
$FeSiAl_4$	–

the m/p interface [11, 12] caused by the high hydrostatic tension generated in the matrix adjacent to the reinforcing particles. Therefore, the mechanical properties of the interface between the alumina particles and the matrix play an important role in determining the positions of voids. The percentage of debonded particles increased significantly by 14% when the test temperature was raised from 25 °C to 180 °C and the

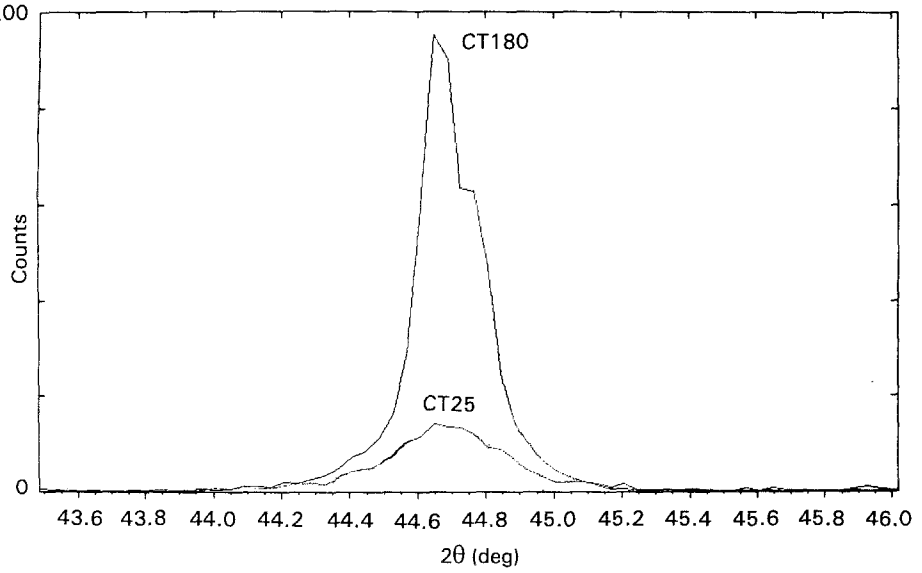

Figure 9 Comparison of the XRD diffraction peaks of spinel in specimens fractured at 25 and 180 °C.

primary void size increased by 22% (see Table I). The different mechanical properties and the increased ductility of the matrix at elevated temperature may be responsible for the higher percentage of debonded particles at 180 °C compared to ambient temperature. A weak interface will promote matrix/particle debonding but a strong interface will enhance particle fracture. Thus, the properties of the m/p interface will play an important role in the deformation and fracture processes [9].

In the present study, the results of EDS line analysis and XRD revealed that the interface layer consisted of spinel in addition to some age-hardening precipitates found in the reaction zones (of the CT25 and CT180 specimens). A spinel layer at the interface of an Al_2O_3-reinforced 6061 Al matrix composite has also been observed by other investigators [8, 13, 14]. High-resolution scanning electron micrographs and EDS line analysis showed some differences in the interface layer thickness of the CT25 and CT180 specimens. XRD analysis also indicated that the amounts of spinel and Mg_2Si are higher in the CT180 specimen. Although the time at elevated temperature was short (about 1 h) for the CT180 specimen, because of the high diffusion rate of elements in MMCs [15], there is the possibility of reactions between matrix and particles occurring, or between elements existing at the interface to form more spinel or age-hardening precipitates. Thermodynamic calculations have shown [14] that Al_2O_3 is not stable in liquid aluminium alloys that contain magnesium, the reaction between Al_2O_3 and solid alloy can occur. Reactions in the solid state, between the matrix and the reinforcement phase have been observed by Suganuma *et al.* [16] and Watanabe and Saitoh [17]. Two possible reactions at this stage are the interaction of the particulate with the matrix and the ageing reaction of elements. These are described below.

4.1. Reaction of particulate reinforcement with matrix

Because the particulate is composed of mullite and alumina, and the matrix contains magnesium, several important reactions are possible. i.e. Reaction 1 [8], and Reaction 2 [8, 13, 14]

$$Al_6Si_2O_{13} + Mg + 2Al = MgAl_2O_4 + 3Al_2O_3 + Si \quad (1)$$

$$4Al_2O_3 + 3Mg = 3MgAl_2O_4 + 2Al \quad (2)$$

Both of these reactions produce spinel, thus the thicker m/p interface at 180 °C could be produced by either or both reactions. The volume change, ΔV, due to these reactions calculated according to

$$(V_{product} - V_{reactants})/V_{reactants} \quad (3)$$

gives values of -16.7×10^{-2} and -4.27×10^{-2} for Reaction 1 and 2, respectively, indicating a volume contraction. This volume contraction will set up tensile radial and hoop stresses in the alumina particles and compressive stresses in the matrix. Such tensile stresses may have resulted in m/p interface separation ahead of the crack tip and hence promoted primary void formation. This therefore explains why there is more interface debonding and larger voids at 180 °C than at 25 °C by separation of the m/p interface.

4.2. Ageing reaction

Solid solution 6061 aluminium alloys containing magnesium and silicon elements is not stable at ambient or elevated temperature. Therefore, a second phase Mg_2Si [18, 19] will eventually precipitate from the supersaturated solid solution. A previous study on Comral-85 showed how the reinforcement phase affects the ageing reaction kinetics and accelerates the ageing process [20]. The observation of some precipitation at the m/p interface of CT25 and CT180 specimens is consistent with these results. The small age-hardened particles at the m/p interface reduce the interface strength. Therefore, the easy nucleation of voids at the m/p interface may be related to these precipitated particles.

On the other hand, magnesium, silicon and probably some other elements which can react or segregate

at the m/p interface leaving a region of the matrix around the particles with low solute levels, may reduce the matrix strength in these regions. In turn, this will affect the load transfer capabilities of the matrix to the particles and aid the process of void formation at the m/p interface.

5. Conclusions

1. The tensile strength, yield strength and elastic modulus of Comral-85 (T6 condition) are found to decrease with temperature from 25–180 °C, while the elongation to failure shows the opposite trend. The fracture toughness, K_{Ic}, increases by 8% from 18.7 MPa $m^{1/2}$ at room temperature to 20.2 MPa $m^{1/2}$ at 180 °C, indicating that it is relatively insensitive to temperature.

2. Examination of the fracture surfaces of Comral-85 has revealed that ductile fracture is the predominant failure mode for all temperatures up to 180 °C. The importance of the m/p interface is shown to increase with increasing temperature. Failure occurs at elevated temperatures by separation of particles from the m/p interface and by plastic flow of the matrix.

3. A reaction zone layer around the Al_2O_3 particles is found to consist of $MgAl_2O_4$ and fine age-hardened precipitates, the amount of which vary with test temperature.

Acknowledgements

The authors thank the Australian Research Council (ARC) Small Grants Scheme for the continuing support of this work. The materials were supplied for testing by Comalco Research Centre, Thomastown, Australia. The authors gratefully acknowledge the assistance of A. Sikorski with the SEM and XRD studies, as is the provision of facilities by the Electron Microscope Unit of the University of Sydney.

References

1. T. G. NIEH, K. XIA and T. G. LANDON, *J. Eng. Mater. Technol.* **110** (1988) 77–82.
2. S. F. CORBIN and D. S. WILKINSON, in "Proceedings of Ceramic and Metal Matrix Composites" edited by R. B. Bhagat, A. H. Clauer, P. Kumar and A. M. Ritter (TMS, Warrendale, PA, 1990) pp. 401–11.
3. B. P. SOMERDAY, Y. LENG, F. E. WAWNER and R. P. GANGLOFF, "Advanced Metal-Matrix Composites for Elevated Temperature" (ASM, Metal Park, OH, 1991) pp. 167–82.
4. A. F. WHITEHOUSE and T. W. CLYNE, in "Proceedings of ICCM/9", Vol. I, edited by A. Miravete, University of Zaragoza (Woodhead Publishing, Madrid, 1993) pp. 393–400.
5. E. FITZER, *Pure. Appl. Chem.* **60** (1988) 287.
6. W. H. KIM, M. J. KOCZAK, and A. LAWLEY, in "Proceedings of the 2nd International Conference on Composite Materials, Toronto, Ontario (TMS-AIME, Warrendale, PA, 1987) pp. 487–505.
7. M. J. HADIANFARD, J. C. HEALY and Y. W. MAI, *J. Mater. Sci.* **28** (1993) 6217.
8. J. DRENNAN, K. XIA and M. J. COUPER, in "Proceedings of Advance Composites '93", edited T. Chandra and A. K. Dhingra, Wollongong, Australia, TMS, (1993) pp. 1015-19.
9. N. HAN, G. POLLARD and R. STEVENS, *Mater. Sci. Technol.* **8** (1992) 184.
10. J. A. ISAACS and A. MORTENSEN, *Metall. Trans.* **23** (1992) 1207.
11. S. R. NUTT and A. NEEDLEMAN, *Scripta Metall.* **21** (1987) 705.
12. T. CHRISTMAN, A. NEEDLEMAN, S. R. NUTT and S. SURESH, *Mater. Sci. Eng.* **A107** (1989) 49-61.
13. C. G. LEVI, G. J. ABBASCHIAN and R. MEHRABIAN, *Metall. Trans.* **9A** (1978) 697.
14. A. D. McLEOD and C. M. GABRYEL, *ibid.* **23A** (1992) 1279.
15. I. DUTTA and D. L. BOURELL, *Acta Metall. Mater.* **38** (1990) 2041.
16. K. SUGANUMA, T. OKAMOTO, T. HAYAMI, Y. OKU and N. SUZUKI, *J. Mater. Sci.* **23** (1988) 1317.
17. H. WATANABE and T. SAITOH, *Keikinzoku* **39** (1989) 262.
18. C. ATONIONE, F. MARRINO, G. RIONTNO, S. ABIS and E. DIRUSSO, *Mater. Chem. Phys.* **20** (1988) 13.
19. C. BADINI, F. MARINO and A. TOMASI, *J. Mater. Sci.* **26** (1991) 6279.
20. M. J. HADIANFARD, Y. W. MAI and J. C. HEALY, *ibid.* **28** (1993) 3665.

Received 2 February
and accepted 6 February 1994